Anal. Bioanal. Electrochem., Vol. 14, No. 9, 2022, 837-845

Analytical & Bioanalytical Electrochemistry

Full Paper

Superparamagnetic Nanoparticles Doped with Lanthanum by Electrochemical Method for Biomedical Applications

Mohammad Rahim Talebtash,[1] and Isa Karimzadeh[2,*]

[1]Department of Engineering, Shahriar Branch, Islamic Azad University, Shahriar, Iran
[2]Department of Physics, Faculty of Science, Central Tehran Branch, Islamic Azad University, Tehran, Iran

*Corresponding Author, Tel.: +98214411009
E-Mail: isa.Karimzadeh@gmail.com

Received: 18 June 2022 / Received in revised form: 20 September 2022 / Accepted: 24 September 2022 / Published online: 30 September 2022

Abstract- In this paper, well-distributed Lanthanum-doped Superparamagnetic nanoparticles (La-Fe_3O_4) are reported. Nanoparticles powder has been synthesized using cathodic electrochemical deposition method. By applying a constant current density of 1 A in a two-electrode electrochemical system, nanoparticles with a diameter of approximately 11 nm with a spherical structure were prepared. The structure, morphology and magnetic properties of these nanoparticles have been systematically investigated by using TEM, XRD, VSM and FT-IR analysis. The results indicate the existence of a superparamagnetic behavior at room temperature for progressive measurements as a function of the magnetic field. The magnetic hysteresis (magnetic saturation, Coercivity and Remanence) of the sample shows the effective role of doped lanthanum in improving the magnetic properties of ferrite nanoparticles, and the magnetic saturation value is 54.23 emu/g. Based on these results, the electrochemical method can be used as an efficient and low-cost synthetic method to make iron oxide nanoparticles doped with lanthanum.

Keywords- Magnetite particles; Iron oxide; Lanthanum-doped; Magnetic saturation; Coercivity; Electrosynthesis

1. INTRODUCTION

Recently, magnetic nanoparticles (MNPs) have become proper candidates for biomedical application due to their important physicochemical capabilities such as suitable magnetic characteristic, simple coat fabrication, colloidal stability, low toxicity. Because of the outstanding properties, there is an astonishing interest in using MNP for medical applications such as magnetic resonance imaging [1-3], cell manipulation [4], hyperthermia [5], targeted drug delivery [6,7], cancer diagnosis [8-10], gene therapy [11,12].

The most common used iron oxides nanostructures are: Fe_3O_4, α-Fe_2O_3 (hematite) and γ-Fe_2O_3 (maghemite). Super paramagnetic iron oxides are interesting field of research due to the natural abundance, low toxicity and great compatibility with the environment and low costs production.

In general, top-down and bottom-up approaches are two main techniques for synthesizing MNPs. Top-down approaches involve breaking up the initial material to produce MNPs by physical methods such as ball milling, electron beam lithography, etc. Bottom-up approaches require the creation of MNPs from their molecules by using both chemical and biological methods such as electrochemical deposition, co-precipitation, solvothermal and hydrothermal [13-19].

Although physical methods are scalable, cost-effective and capable of industrial production, in some methods, such as the steam condensation method, they have disadvantages such as exothermicity and oxidation. Also, a significant amount of mechanical, thermal or electrical energy is needed to transform materials into nanoparticles. The chemical methods have a higher capability due to better control of synthesized parameters (temperature, molar ratio of raw materials, pH). So, the chemical method has a unique ability in the field of technology and science of nanostructured materials due to the arrangement of materials in nanometer conditions in order to achieve the desired properties.

Among the mentioned approaches, the electrochemical method based on the process of iron oxidation is considered as efficient method, due to simplicity of the synthesis stage, room temperature, high performance, low cost and compatibility with the environment. These characteristics referred to the simple controlling parameters such as voltage, current, temperature concentration, and pH applicable in the deposition experiments.

Due to their magnetic properties, magnetite nanoparticles tend to adsorb each other and it results unwanted agglomeration [20-22]. Agglomeration of iron oxide nanoparticles is the main challenge because by agglomeration the specific surface area of iron oxide nanoparticles decreases and cussed malfunction of magnetic properties nanoparticles and in the presence of a magnetic field, their performance is significantly reduced. Moreover, the specific surface area of magnetite nanoparticles reduced due to their adhesion and also load-bearing capacity of the active material in heavy metal as well as catalytic applications decrease and makes them difficult to apply. a proper solution for these problems is doping some element like Lain to the

magnetite particles. This approach increases the intensity of magnetization and thus reduces the tendency of nanoparticles to stick together.

In this paper, we used electrochemical approach to synthesizing La-doped Fe_3O_4 MNPs. In this method, the agglomeration tendency of the nanoparticles is less. On the other hand, the size of the nanoparticles can be controlled by applying oxidation current density or potential to the system.

2. EXPERIMENTAL

2.1. Materials

Ferrous chloride tetrahydrate ($FeCl_2 \cdot 4H_2O$) (%99), ferric chloride hexahydrate ($FeCl_3 \cdot 6H_2O$) (%99), Lanthanum Chloride Heptahydrate ($LaCl_3 \cdot 7H_2O$), Sodium hydroxide (%98), Ammonium solution (25%), chloric aside (%37) and distilled water, have been used for synthesizing pure and doped MNPs. The materials were purchased from Merck, Germany.

2.1.1. Synthesis of La-Doped Fe3O4

The sample was fabricated using the novel cathodic electrodeposition method which is reported in several publishes [23,24]. One litter electrolyte of 3 g ($FeCl_3 \cdot 6H_2O$), 1.5 g $FeCl_2 \cdot 4H_2O$ chloride and 0.5 g ($LaCl_3 \cdot 7H_2O$) dissolved in ethanol was prepared and stirred with a magnet for 30 min.

By using a DC power source, a current density of 0.1 A/cm^2 was applied to the bath cell for 10 minutes, and then a black thin film was observed on the cathode electrode. Then the electrode was removed from the electrolyte and washed several times with ethanol. The observed film was scratch from the surface of the steel electrode and then the obtained powder was dried at 80 °C RT for 5 h.

In the aqueous environment, the formation of La-Fe_3O_4 on the cathode surface occurs through a two-stage electrochemical-chemical mechanism:

Electrochemical stage: In this stage, as a result of cathodic reactions, base (OH) is produced on the cathode surface.

$$2H_2O + 2e^- \rightarrow H_2 + 2OH^- \quad (1)$$

Cathodic reactions cause a local increase in pH on the electrode surface, in fact, these two reduction reactions cause an increase in the pH of the electrolyte at the electrode-electrolyte interface by producing -OH. These reactions compete with metal reduction reactions.

$$Fe^{3+} + e^- \rightarrow Fe^{2+} \quad (2)$$

Chemical stage: In this stage, OH^- produced on the surface of the cathode reacts with metal cations and deposits are formed:

$$(1-x)Fe^{2+} + x\,La^{3+} + 2Fe^{3+} + 6OH^{-} \rightarrow Fe(II)_{(1-x)}La_x\,Fe(III)O_4 + 3H_2O \qquad (3)$$

2.2. Characterization techniques

The elemental composition of MNPs was examined through X-ray diffraction (XRD), and data with 2θ in the angle range (15 °-70 °) with the type X-Pert Pro MPD, Cu-Kα (λ = 1.54060 A °) recorded. The transmission of the optical spectrum in the infrared spectrum (FTIR) was performed at the range of $400-4000\,cm^{-1}$ by a spectrum RXI infrared Fourier transform spectrometer manufactured by Perkin Elmer. The appearance and average size of MNPs were determined by transmission electron microscopy (TEM) with Zeiss EM-900 model (80 kv). The magnetic behavior of the samples was evaluated by a vibrating sample magnetometer (VSM) with Lake Shore 7400 model at room temperature

3. RESULTS AND DISCUSSION

3.1. Morphological observation by TEM

Morphological images of doped sample provided by TEM instruments. Figure 1 is shown the spherical colonies of fine Lithium doped iron oxide particles. The observed particles are completely uniform spheres with a size of about 11.1 nm. Some of MNPs form multiparticle aggregates, probably due to magnetic dipole interparticle interactions.

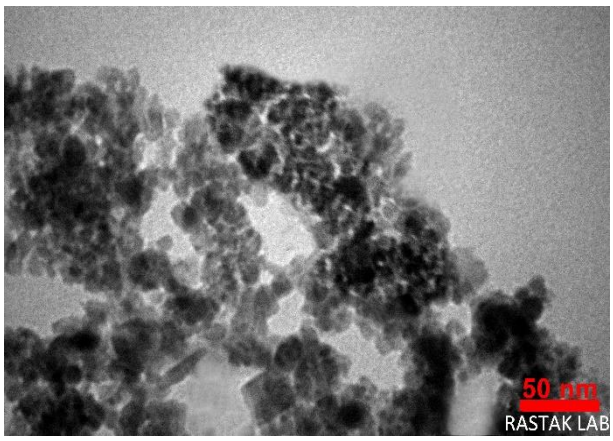

Figure 1. TEM analysis of La-Fe_3O_4

3.2. Magnetic properties by VSM

The magnetic characteristics of the prepared MNPs were measured using a vibrating sample magnetometer (VSM). Figure 2(a) shows the diagrams of MNPs in which magnetic saturation has occurred in the external field and re-plotted at the small applied fields in Figure 2(b) to calculate the number of quantities positive (and negative) Mr and Ce and listed in Table 1. S-like form confirms that the hysteresis is almost negligible and the remanence (Mr) and

coercivity (Ce) are very small (i.e., $Mr = 1.05$ emu/g and $Ce = 9.98$ Oe), which confirmed the behavior of superparamagnetic.

These magnetization values indicate the suitable performance of the fabricated MNPs at the external field, and higher than the necessary threshold for biomedical aims like drag delivery, hyperthermia and MRI contrast agent [25-29]. Also, the negligible Mr and Ce value of this fabricated MNPs revealed its suitable superparamagnetic nature for the biomedical aims.

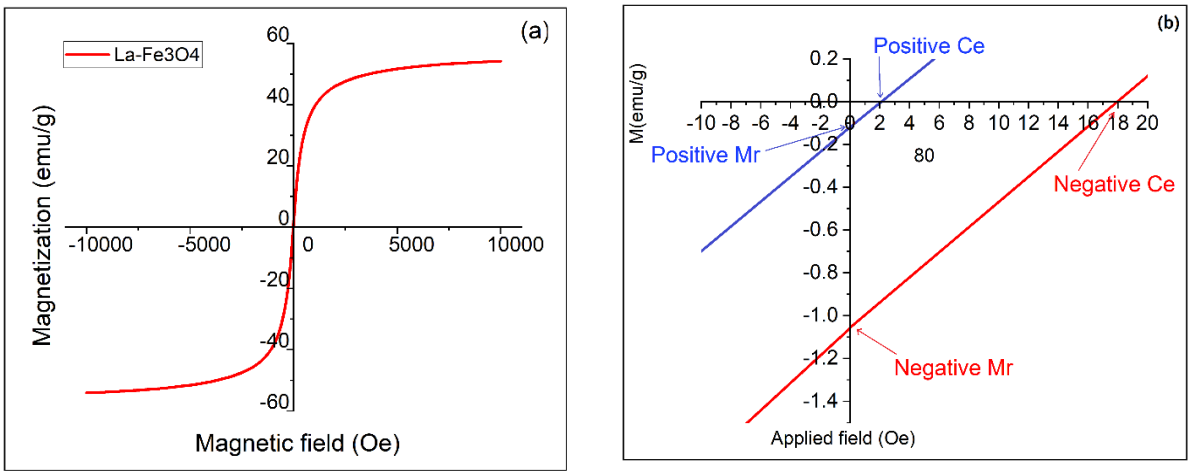

Figure 2. (a) The measured M-H profile for the deposited IONs and (b) their hysteresis loop at the conditions of applied field →0

Table 1. Magnetic parameters measured through VSM analysis

Sample	Ms (emu/g)	Coercivity (Oe)	Remanence (emu/g)	Negative Mr (emu/g)	Positive Mr (emu/g)	Positive Ce (Oe)	Negative Ce (Oe)
$La\ Fe_3O_4$	54.23	9.98	0.59	-1.05	-0.12	2.00	17.95

The MNPs size can also be calculated from VSM curve by using Langevin's formula [30]:

$$D_m = \left(\frac{18\ k_B T\ x_i}{\pi\ \rho\ M_s}\right)^{\frac{1}{3}} \quad (4)$$

where ρ is the density of Fe_3O_4 (5.18 g/cm^3), χ_i is initial susceptibility (emu/g), T is (300 k), and k_B is Stefann Boltzman's constant ($1.38 \times 10^{-23}\ J/K$) and according to Table 1, 31.79 emu/g.

The mean MNPs size was calculated 9.8 nm which is smaller than the TEM measurement. As alternative mechanisms can lead to particle demagnetization, the simplest assumption was

that the surface layer of magnetized atoms does not contribute to the particle's magnetic properties. Therefore, the magnetic "dead layer" [31] on the particle surface explains the difference between D_m and D_{TEM}.

3.3. Structure analysis by XRD and FT-IR

The X-ray diffraction pattern was investigated using XRD technique and also the diffraction lines were indexed and is the result depicted in Figure 3. The peak patterns are completely in agreement with the JCPDS card number 01-088-0315. The crystal plane (111), (220), (311), (400), (422), (511), (440) and (533) are clearly visible in the pattern which confirm the successful synthesize of crystalline Li-Fe_3O_4 with single-phase cubic reverse spinel. Moreover, no additional peaks are observed which proved the purity of the fabricated sample.

From reference peak (311), the size of the MNPs (D) was calculated by Scherer's Eq. [32]:

$$d = \frac{0.9\,\lambda}{\beta \cos\theta}$$

The crystallite size of doped MNPs was about 8.5 nm.

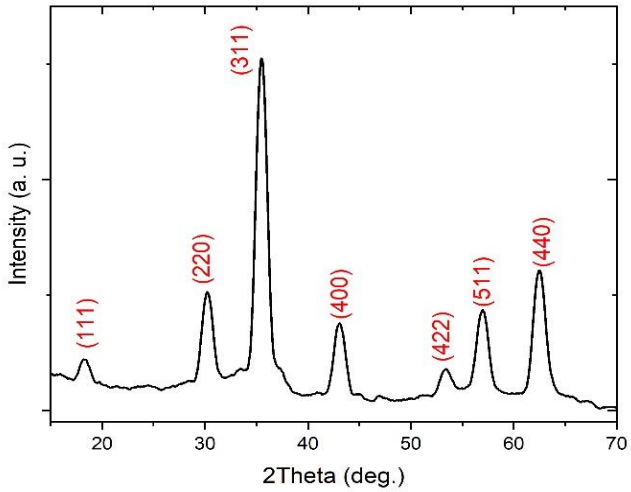

Figure 3. XRD pattern of the $La - Fe_3O_4$ sample

Also, to characterize the phase and composition of MNPs, FTIR analysis was performed and illustrated in Figure 4. The main identified bands are located at 575-659 cm^{-1} which represent split of the $\nu 1$ vibrations band of the Fe-O/La-O bonds [33,34]. The absorption band in the range of 3440 cm^{-1} is due to the strong stretching vibration of the hydrogen bond within H-O hydroxyl groups. The bands at 2856 and 2926 cm^{-1} are related to $\nu_{asy.str.}$ of CH_2 groups [35,36]. The bands located at 1636, 1117 and 1020 cm^{-1} are due to $\nu_{str.}$ of C=O, C-O and C-N groups, respectively [34,35].

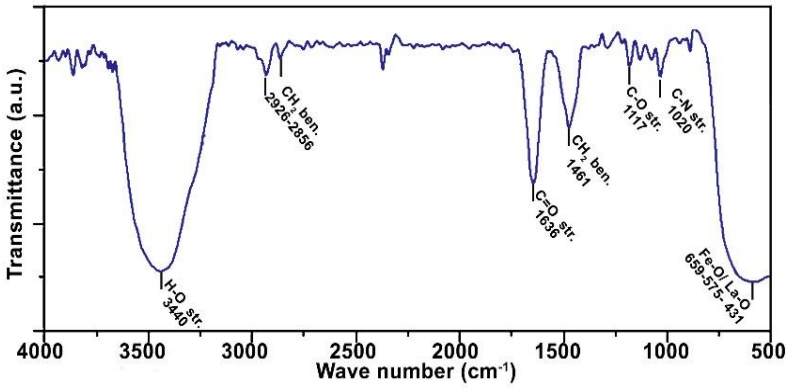

Figure 4. FTIR pattern of the $La-Fe_3O_4$ sample

4. CONCLUSIONS

In this work, La-doped iron oxide nanoparticles with magnetite phase in aqueous electrolyte solution were prepared by a one-step cathodic electrochemical precipitation**.** Morphological observations through TEM showed that La-Fe_3O_4 nanoparticles are well dispersed and have no agglomerate state and the average particle size was about 11.1 nm. MNPs have a good supermagnetic behavior and Ms=54.23 emu/g, Ce=9.98 Oe and Mr=0.59 emu/g. Finally, proposed that La-Fe3O4 nanoparticles have high potential for biomedical applications. However, before using these MNPs in biomedical applications, some key characteristics should be investigated: molecular length and weight, chemical structure, structure, binding mechanism to the particle surface (covalent, hydrophobic or ionic bond).

REFERENCES

[1] R. Qiao, C. Yang, and M. Gao, J. Mater. Chem. 19 (2009) 6274.

[2] Y. Wang, C. Xu, Y. Chang, L. Zhao, K. Zhang, Y. Zhao, F. Gao, and X. Gao, ACS Appl. Mater. Interfaces 9 (2017) 28959.

[3] H. Li Chee, C. Ruey R. Gan, M. Ng, L. Low, D. G. Fernig, K. K. Bhakoo, and D. Paramelle, ACS Nano, Article ASAP (2018) 07572.

[4] S. Moise, E. Céspedes, D. Soukup, J. M. Byrne, Alicia J. El Haj, and N. D. Telling, Sci. Rep. 7 (2017) 39922.

[5] G. Kandasamy, A. Sudame, T. Luthra, K. Saini, and D. Maity, ACS Omega 3 (2018) 3991.

[6] M. Magro, D. Baratella, E. Bonaiuto, J. Almeida Roger, G. Chemello, S. Pasquaroli, L. Mancini, I. Olivotto, G. Zoppellaro, J. Ugolotti, C. Aparicio, A. P. Fifi, G. Cozza, G. Miotto, G. Radaelli, D. Bertotto, R. Zboril, and F. Vianello, Biomacromol. 20 (2019) 1375.

[7] A. Ali, H. Zafar, M. Zia, I. Ul Haq, A. R. Phull, J. S. Ali, and A. Hussain, Sci. Appl. 9 (2016) 49.

[8] K. Li, H. Nejadnik, and H. E. Daldrup-Link, Drug Discovery Today 22 (2017) 1421.
[9] B. M. Geilich, I. Gelfat, S. Sridhar, A. L. van de Ven, and T. J. Webster, Biomaterial 119 (2017) 78.
[10] P. O. Champagne, H. Westwick, A. Bouthillier, and M. Sawan, Nanomedicine 13 (2018) 1385.
[11] X. C. Zheng, W. Ren, S. Zhang, T. Zhong, X. C. Duan, Y. F. Yin, and M. Q. Xu, Int. J. Nanomed. 13 (2018) 1495.
[12] F.B. Effenberger, R. A. Couto, and P.K. Kiyohara, Nanotechnology 28 (2017) 115603.
[13] V. Patselas, L. Kosinová, M. Lovri, L. Ferhatovic, M. Rabyk, and et al., ACS Appl. Mater. Interfaces 8 (2016) 7238.
[14] M. Aghazadeh, I. Karimzadeh, M.G. Maragheh, and M.R. Ganjali. Mater. Res. 21 (2018) e20180094.
[15] M. Farahmandjou, and S.A. Salehizadeh, Glass Phys. Chem. 39 (2013) 473.
[16] E. L. Albert, C. A. Che Abdullah, and Y. Shirataki, Results Phys. 11 (2018) 944.
[17] M. Farahmandjou, S. Honarbakhsh, S. Behrouzinia, Phys. Chem. Res. 4 (2016) 655.
[18] A. Ali, S. Rehmat, P. Zhou, K. Guo, M. Ovais, and M. Rehmat, Front. Chem. 9 (2021) 629054.
[19] A. Khodadadi, M.R. Talebtash, M. Farahmandjou, Phys. Chem. Res. 10 (2022) 537.
[20] J.A. Fuentes-García, A.I. Diaz-Cano, A. Guillen-Cervantes, and et al., Sci. Rep. 8 (2018) 5096.
[21] X. Yu, G. Cheng, and S. Y. Zheng, Sci. Rep. 6 (2016) 25459.
[22] I. Karimzadeh, Anal. Bioanal. Electrochem. 10 (2018) 631.
[23] M. Aghazadeh, I. Karimzadeh, M.R. Ganjali, and A. Malekinezhad, Int. J. Electrochem. Sci. 12 (2017) 8033.
[24] I. Karimzadeh, M. Aghazadeh, T. Doroudi, M.R. Ganjali, and P.H. Kolivand, Mater. Research Innovations 22 (2018) 352.
[25] D. E. Lee, H. Koo, I. C. Sun, J. H. Ryu, K. Kim, and I. C. Kwon, Chem. Soc. Rev. 41(2012) 2656.
[26] J. J. Giner-Casare, M. Henriksen-Lacey, M. Coronado-Puchau, and L. M. Liz-arzan, Mater. Today 19 (2016) 19.
[27] R. M. Patil, P. B. Shete, N. D. Thorat, S. V. Otari, K. C. Barick, A. Prasad, R. S. Ningthoujam, B. M. Tiwale, and S. H. Pawar, J. Magn. Magn. Mater. 355 (2014) 22.
[28] M. Aghazadeh, I. Karimzadeh, and M. R. Ganjali, Curr. Nanosci. 15 (2019) 169.
[29] N. V. Srikanth Vallabani, and S. Singh, Biotech. 8 (2018) 279.
[30] Z.L. Liu, Y.J. Liu, K.L. Yao, et al. J. Mater. Synthesis and Processing 10 (2002) 83.
[31] R. Kaiser, and G. Miskolczy, J. Appl. Phys. 41 (1970) 1064.
[32] P. Scherrer, Bestimmung der inneren Struktur und der Größe von Kolloidteilchen mittels Röntgenstrahlen, Mathematisch- Physikalische Klasse 2 (1918).

[33] I. Karrimzadeh, and M. Faryadi, Anal. Bioanal. Electrochem. 11 (2019) 657.
[34] D. Sivakumar, M. M. Rafi, B. Sathyaseelan, K. M. Prem Nazeer, and A. M. Ayisha Begam, Int. J. Nano Dimens. 8 (2017) 257.
[35] I. Karimzadeh, M. Aghazadeh, T. Doroudi, M. R. Ganjali, P. H. Kolivand, and D. Gharailou, Curr. Nanosci. 13 (2017) 274.
[36] I. Karimzadeh, M. Aghazadeh, M. R. Ganjali, P. Norouzi, T. Doroudi, and P. H. Kolivand, Mater. Lett. 189 (2017) 290.